Mechanisms of autogenous shrinkage for Ultra-High Performance Concrete (UHPC) prepared with pre-wet porous fine aggregate (PFA)

Journal of Building Engineering 54 (2022) 104622

Contents lists available at ScienceDirect

Journal of Building Engineering

journal homepage: www.elsevier.com/locate/jobe

Mechanisms of autogenous shrinkage for Ultra-High Performance Concrete (UHPC) prepared with pre-wet porous fine aggregate (PFA)

Kaizhi Liu [a,b], Yong Long [a], Luyi Chen [a], Xuan Ling [c,*], Rui Yu [b,**], Zhonghe Shui [b], Shunxin Fei [a,d], Wenzhi Yu [a], Chen Li [a], Keyu Ge [a]

[a] State Key Laboratory for Health and Safety of Bridge Structures, China Railway Major Bridge Engineering Group Co., Ltd, Wuhan, 430034, PR China
[b] State Key Laboratory of Silicate Materials for Architectures, Wuhan University of Technology, Wuhan, 430070, PR China
[c] Department of the Built Environment, Eindhoven University of Technology, P.O. Box 513, 5600 MB, Eindhoven, the Netherlands
[d] School of Materials Science and Engineering, Anhui University of Technology, Maanshan, 243002, PR China

ARTICLE INFO

Keywords:
Ultra-High Performance Concrete (UHPC)
Autogenous shrinkage
Expansion
Internal relative humidity (IRH)
Internal temperature (IT)

ABSTRACT

Here, the intrinsic driving mechanisms of autogenous shrinkage for Ultra-High Performance Concrete (UHPC) incorporating porous internal curing (IC) medium are detailly investigated, including characterization and monitoring of UHPC hydration kinetics, internal relative humidity (IRH) and internal temperature (IT) fields. The results show that the autogenous shrinkage evolution of UHPC prepared with pre-wet porous fine aggregate (PFA) undergoes multiple stages. The potential expansion drivers of UHPC with IC at super early hardening period are identified as the extra liquid volume compensation and the effect of thermal expansion. Furthermore, the rapid shrinkage growth stage of the UHPC matrix is governed by the hydration dynamic, while the sustained shrinkage growth stage is managed by cold shrinkage, chemical shrinkage and capillary pressure. Finally, the feasibility of the *Powers* model in the design of UHPC incorporating wet PFA is carefully revealed, and the key parameters for obtaining UHPC with advanced volumetric stability are elucidated. The strategy in terms of the autogenous shrinkage for the UHPC designed with PFA is revealed.

1. Introduction

Ultra-High Performance Concrete (UHPC) is a new favored construction material with exceptional mechanical properties and durability, designed on the basis of a high packing density of solid mixture particles and an extremely low water-binder ratio (usually w/b < 0.25) [1–4]. Nevertheless, the high dosage of cementitious materials used in UHPC has led to rapid shrinkage development and matrix volume reduction at an early age [4–11]. The generation and extension of micro-crack within the matrix caused by shrinkage stresses reduce the mechanical properties and corrosion resistance of UHPC. Severe cracks exist in the UHPC concrete at 7d in Fig. 1. Hence, how to effectively mitigate the early shrinkage deformation of UHPC is one of the significant research topics of UHPC in recent years.

* Corresponding author.
** Corresponding author.
E-mail addresses: x.ling@tue.nl (X. Ling), r.yu@whut.edu.cn (R. Yu).

https://doi.org/10.1016/j.jobe.2022.104622
Received 22 March 2022; Received in revised form 25 April 2022; Accepted 4 May 2022
Available online 9 May 2022

Typically, the early volume deformation of concrete is influenced by chemical shrinkage, thermal deformation and autogenous shrinkage [12]. But, for UHPC with lower hydration, the early chemical shrinkage and thermal deformation lead to a relatively small proportion, compared to the development of autogenous shrinkage [10,13–16]. Current theories involved in the generation and evolution mechanisms of autogenous shrinkage in concrete include theories of surface tension [17,18], disjoining pressure [19] and capillary tension [20,21] et al. As widely accepted, autogenous shrinkage can be attributed to the consumption of free water and its migration within the concrete matrix. In addition, the increase in depression of the meniscus in the capillary pores caused by the self-desiccation effect induces a reduction in the apparent volume of the concrete [5,22–25]. Theoretically, both shrinkage-reducing agents [26–29] and internal curing (IC) [30–36] can help to maintain the initial capillary pressure and simultaneously reduce the autogenous shrinkage of UHPC. Some investigations have demonstrated that the use of shrinkage-reducing agents can also reduce the mechanical properties of concrete [37,38].

IC releases the free water during the curing stage to delay the decrease in internal relative humidity (IRH) and the self-desiccation behavior of concrete, which can be considered as the most effective way to inhibit the development of autogenous shrinkage in the UHPC matrix. Currently, the main internal curing agents used for UHPC are super absorbent polymer (SAP), porous active powder, biological fiber, and porous fine aggregate (PFA). The SAP with internal reservoir structures [8,39–41], rice husk ash [42,43], metakaolin [44,45], calcined bauxite [46] and cellulose fiber [47,48] have been reported to significantly reduce the autogenous shrinkage of UHPC, and even cause early-age slight matrix expansion. Nevertheless, the volume contraction of SAP after releasing water may induce extra voids in the interfacial areas between SAP and the matrix, thus increased porosity may reduce the mechanical properties and durability of UHPC [49]. In addition, the porous active powders usually require calcination at high temperatures (over 500 °C), which increases energy consumption and costs [50]. The pretreatment process of biological fibers is complicated, and their stability is questionable. In addition, their poor dispersion severely affects the workability and homogeneity of fresh paste [47,51]. Compared to the three types of IC medium mentioned above, natural PFA can overcome these limitations and deficiencies, thus favored for UHPC applications, such as coral sand [52,53] and pumice [54,55]. The pore structure parameters, particle size distribution, dosage, pre-wetting mode, water absorption state and the total excess water related to IC efficiency of PFA have been intensively investigated.

The usage of PFA in UHPC delays the decline of IRH, which is a widely accepted approach to reduce the autogenous shrinkage. Meng et al. [56] revealed that the early development of autogenous shrinkage in UHPC with the incorporation of saturated PFA correlated well with the decline in IRH. However, the addition of excess saturated PFA has also been reported to increase the autogenous shrinkage of UHPC [54,57]. Valipour et al. [58], Wang et al. [52] and Liu et al. [53] observed micro-expansion of UHPC prepared with saturated PFA after setting, and further study was needed to explain the mechanism of the expansion. The extra free water carried by PFA can compensate for the IRH loss, altering the early hydration behavior of UHPC and thus affecting its shrinkage behavior. Considerable efforts have been made to understand the internal interaction behavior with IC. Liu et al. [57] and Huang et al. [59] found that the IRH of hardened UHPC (with or without IC) does not drop immediately after setting, but remains at saturated humidity for a period of time. However, the shrinkage increases rapidly after setting, indicating that the autogenous shrinkage of UHPC is not only determined by IRH. Shen et al. [60] pointed out that the desorption of water from PFA is a continuous process in UHPC and that only part of the introduced water serves to compensate for the IRH. In addition, excessive PFA content and entrained moisture can severely reduce the strength of the UHPC matrix [52–55,57]. Zhang et al. [61] explained that the autogenous shrinkage behavior of

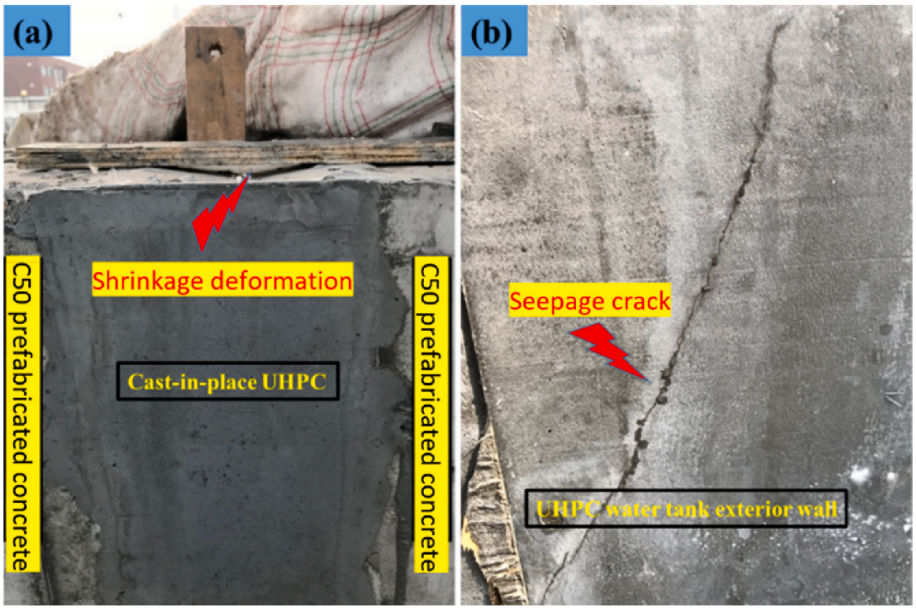

Fig. 1. Shrinkage deformation and cracking risk of UHPC after wet film curing and covered with bedclothes (the authors participated and photographed at 7d):(a) UHPC wet joint; (b) UHPC water tank.

UHPC is multi-stage, as it is controlled by thermal deformation at an early stage and later influenced by hydration reaction. Therefore, the autogenous shrinkage of UHPC is associated with both IRH and hydration process in UHPC [62,63]. Notably, chemical shrinkage overlaps with autogenous shrinkage and is difficult to isolate from the test results. Besides, the heat released during hydration also leads to the generation of temperature gradient and thermal deformation in the matrix [64,65], which also contributes to the development of autogenous shrinkage. It is therefore valuable to reveal the mechanism of these factors in the autogenous shrinkage of UHPC, including the IRH, hydration process, thermal deformation.

The primary objective of this work is to advance the current understanding of the autogenous shrinkage mechanisms of UHPC prepared with various dosages and absorption states of PFA. The evolution of autogenous shrinkage of UHPC was investigated by using multiple materials characterization techniques, including the hydration process, the internal temperature and humidity of the composite cementitious system. Consequently, common PFA was applied in this study to replace part of river sand as the IC agent for UHPC. The mechanisms and multiple driving forces of autogenous shrinkage of UHPC were then investigated in detail. The feasibility of the Powers model is evidenced when applied in the UHPC concrete designed with internal curing. In addition, the desorption behavior of PFA should be considered for the optimal entrained water.

2. Materials and methodologies

2.1. Materials

Ordinary Portland Cement 52.5 (OPC 52.5), fly ash (FA) and silica fume (SF) were utilized as binder materials in this study. Two well-graded natural river sand S-RS (0–0.6 mm) and M-RS (0.6–1.25 mm) were selected as fine aggregates. A kind of crushed coral reef (0–0.6 mm) was employed as a PFA with varying volume replacement of S-RS in UHPC with full saturated water absorption of 31% (wt. %) [66]. The percentage of the PFA needed to offset self-desiccation is 13% by volume according to ASTM C1761. Then the replacement level was set 10%–30% by volume of S-RS. The chemical compositions and physical properties of the binder materials and fine aggregates are listed in Tables 1 and 2. The Scanning Electron Microscope (SEM) images of the pore structure of the used PFA are presented in Fig. 2. The detailed particle size distributions of the raw materials are shown in Fig. 3. In addition, a polycarboxylic-based superplasticizer (≈20% solid contents and >40% water reduction) was employed to ensure a satisfying fluidity.

The pre-wetted PFA was prepared with different water adsorption (19%, 25% and 31% by weight in PFA_1, PFA_2 and PFA_3, respectively). The pre-wetted PFA was then mixed thoroughly and placed in a sealed chamber with 20 ± 2 °C, RH 90 ± 2%, and weighed with an electronic balance. The weight loss of PFA was recorded every 10 min until there was no further change within 30 min. The water desorption rate of PFA was then calculated. Notably, the desorption rate of PFA is varied from the starting water adsorption as shown in Fig. 4. The maximum water release from PFA_1, PFA_2, PFA_3 is 91.1%, 89.0%, 88.2%, respectively.

2.2. Mix design

The modified Andreasen and Andersen (*A&A*) model was applied to optimize the proportions of solid particles in the designed UHPC [52,67]. The mixed water and SP contents were determined considering the workability and homogeneity of the fresh slurry of UHPC (no segregation and bleeding with maximum introduced water in the IC). Finally, the S-RS was replaced by $PFA_{1/2/3}$ at 10%, 20% and 30% by volume in C10, C20 and C30, respectively. Fibers were excluded from this experimental design to avoid their influence on shrinkage behavior [68,69]. Some details of the UHPC mixture design are shown in Table 3. The maximum water desorption from PFA was then used to calculate the actual w/b ratio. Both the total and actual w/b ratio in each mixture of UHPC are listed in Table 4.

2.3. Specimens preparation

The PFA with different starting water adsorption were prepared. Specifically, the calculated water and dry PFA were well mixed and sealed at 20 ± 2 °C for 72 h. The UHPC mixtures in Table 3 were prepared in a mixer. The solid materials including cement, fly ash, silica fume and sand were pre-mixed at 60 rpm for 3 min. The pre-wetted PFA and water containing SP were then added and blended at 120 rpm for a further 90 s. All the fresh samples were cured at room temperature and covered with plastic film for 1d. Then the samples were demolded and cured in water (20 ± 2 °C).

Table 1
Chemical compositions of binder materials and fine aggregates (wt. %).

Oxide	OPC 52.5	FA	SF	RS	PFA
Na_2O	0.08	0.33	0.13	0.22	0.38
MgO	1.62	0.23	0.47	0.12	2.00
Al_2O_3	4.58	38.01	0.25	4.04	0.25
SiO_2	21.28	46.44	94.65	91.67	0.98
P_2O_5	0.12	0.06	0.17	0.03	0.07
SO_3	2.48	0.69	0.69	0.02	0.74
K_2O	0.77	0.88	0.84	2.08	0.03
CaO	65.21	7.50	0.36	0.24	50.42
Fe_2O_3	3.25	3.12	0.15	0.87	0.09
LOI	0.61	2.79	2.29	0.53	44.32

Table 2
Physical properties of binder materials and fine aggregates.

Indicator	OPC 52.5	FA	SF	S-RS	M-RS	PFA
Specific gravity	3.14	2.31	2.20	2.66	2.60	2.57
Median diameter (μm)	12	10	3	446	814	396

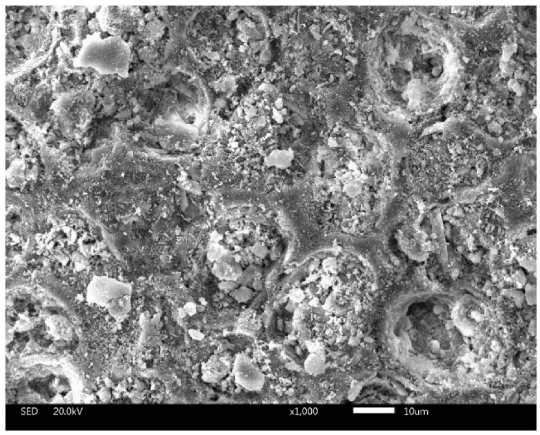

Fig. 2. The SEM images of the employed PFA.

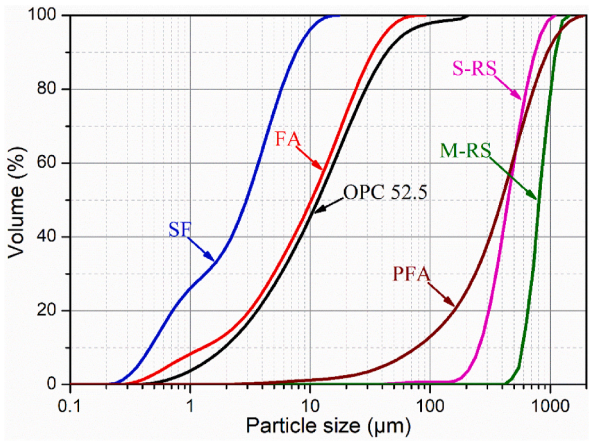

Fig. 3. Particle size distributions of raw materials.

2.4. Test programs

2.4.1. Fresh properties

The Fluidity of fresh UHPC was tested according to ASTM C1437-15. The size of the mini-slump cone is 60 mm in height, and the upper and lower diameters are 70 mm and 100 mm, respectively. The slurry flowed freely on the plate and the average value of the diffusion diameters was recorded as the fluidity.

The setting time of the UHPC mortar was measured using the penetration resistance method, according to ASTM C403. A needle with a bearing area of 20 mm^2 was selected and the test was conducted in a room at 20 ± 2 °C. The initial and final setting time were determined when the penetration resistance was equal to 3.5 MPa and 28 MPa, respectively.

2.4.2. Mechanical properties

The compressive strength of the UHPC specimen was measured according to GB/T17671-1999. The samples were cast in metal molds (40 mm × 40 mm × 160 mm) for 24 h and sealed with a film. After curing in water for 1, 3, 7, 28, 56 d (20 ± 2 °C), six samples for each batch were tested at a loading rate of 2.4 ± 0.2 kN/s.

2.4.3. Autogenous shrinkage

A non-contact method with a volume 5.15L was employed according to the Chinese national standard GB/T 50082-2009 (see

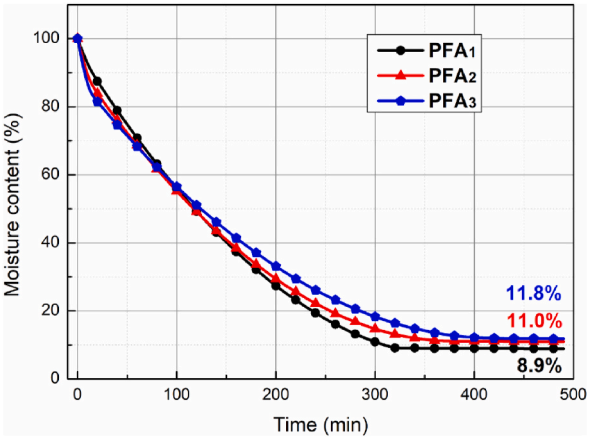

Fig. 4. The desorption rate of PFA with various starting water adsorption.

Table 3
Mix proportion of UHPC combined with wet PFA (kg/m^3).

Num.	OPC 52.5	FA	SF	S-RS	M-RS	Wet PFA	Water	SP
C0	750	200	144	770	220	0	175	31
PFA_1C10	750	200	144	693	220	88	175	31
PFA_1C20	750	200	144	616	220	177	175	31
PFA_1C30	750	200	144	539	220	265	175	31
PFA_2C10	750	200	144	693	220	93	175	31
PFA_2C20	750	200	144	616	220	185	175	31
PFA_2C30	750	200	144	539	220	278	175	31
PFA_3C10	750	200	144	693	220	98	175	31
PFA_3C20	750	200	144	616	220	195	175	31
PFA_3C30	750	200	144	539	220	293	175	31

Table 4
Actual water content and w/b ratio in each group of UHPC.

Num.	Water content (kg/m^3)			w/b ratio		
	Mixing	SP carrying	IC introducing	Net	Total	Actual
C0	175	24.8	0	0.183	0.183	0.183
PFA_1C10	175	24.8	14.1	0.183	0.196	0.195
PFA_1C20	175	24.8	28.2	0.183	0.208	0.206
PFA_1C30	175	24.8	42.4	0.183	0.221	0.218
PFA_2C10	175	24.8	18.4	0.183	0.199	0.197
PFA_2C20	175	24.8	36.7	0.183	0.216	0.212
PFA_2C30	175	24.8	55.1	0.183	0.233	0.227
PFA_3C10	175	24.8	23.2	0.183	0.204	0.201
PFA_3C20	175	24.8	46.4	0.183	0.225	0.220
PFA_3C30	175	24.8	69.6	0.183	0.246	0.238

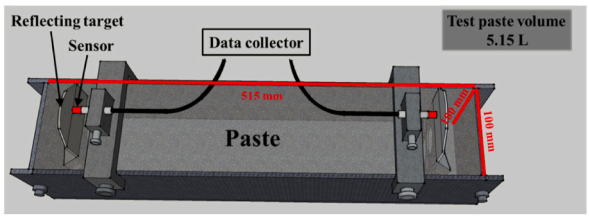

Fig. 5. 3D structural diagrams of the used non-contact device for UHPC autogenous shrinkage measurement.

Fig. 5). Fresh samples were cast into molds (100 m × 100 m × 550 m) and sealed with two layers of polyethylene sheets. The test temperature was controlled at 20 ± 2 °C and the final setting time was defined as the "Time Zero" for autogenous shrinkage.

2.4.4. Hydration products

X-ray Diffraction (XRD) and thermo-gravimetric (TG) tests were conducted to analyze the phase composition and hydration products of UHPC. After 5 h curing, several pieces were obtained from the center of the specimen, ground and sieved, and then dried at 60 °C. The samples were tested using a D8 Advance instrument with a step size of 0.02° and a 2θ range of 5°–20° (Cu-Kα, 1°/min). Thermo-gravimetry of the samples was conducted using a STA449F3 instrument at a 10 K/min heating rate from 20 °C to 1000 °C under nitrogen atmosphere.

2.4.5. Internal humidity and temperature fields

As seen in the 3D illustration of the test device in Fig. 6, a cube sample with a dimension of 100 mm × 100 mm × 100 mm was cast and sealed with a membrane. In the center of the exposed surface of the specimen, a hollow duct that can be dredged at the bottom was inserted, with a depth of 50 mm. After the slurry loses its plasticity, open the bottom of the catheter and a small thin mesh cluster is inserted into the catheter. A probe that can monitor and record humidity and temperature is inserted from the duct to bring the sensor area into contact with the mesh cluster. The probe (HMT337, Vaisala) measures humidity and temperature with an accuracy of 0.1% and 0.1 °C respectively.

2.4.6. Hydration process

Isothermal calorimetry (TAM Air) was employed to reveal the effect of different PFA entrained water contents on the hydration process of UHPC. Nearly 20 g of mortar samples of each recipe were prepared and tested at 20 ± 0.1 °C for 7 days. Heat flow and cumulative heat were recorded and normalized by the mass of the solid binder.

3. Results and discussions

3.1. Fresh properties

As the UHPC mixtures are prepared with different dosages of PFA and the PFA is used with different water adsorption state, the water to binder ratio in each mixture is calculated as Eq. (1) and Eq. (2).

$$w = \frac{M_W + M_S + M_P}{M_b} \tag{1}$$

$$M_p = M_{PFA} \times \alpha \tag{2}$$

where w, M_W, M_S, M_P, M_b, M_{PFA} and α are the water to binder ratio, the mass of additional free water, the mass of water form SP, the mass of the biner, the mass of water released from PFA, mass of water stored in PFA and the desorption rate of PFA, respectively.

The fluidity and setting time of fresh UHPC prepared with or without PFA are listed in Table 5. The wet PFA significantly improves the workability of UHPC. The flowability of fresh UHPC slurry is positively correlated with the actual w/b ratio of the reaction system in Fig. 7. Some similar results have been reported elsewhere [56,60], as free water stored in the pores of the PFA is released in the mortar during the mixing process. The released water can improve its workability.

The setting time of UHPC is particularly critical for assessing the autogenous shrinkage of the UHPC matrix, which is deemed to be related to the formation of the gels. Similar initial and final setting time can be observed for each mixture. The final setting will occur within 30–90 min after the initial setting. With the exception of PFA_1C10, the initial and final setting time of UHPC containing PFA are prolonged, indicating that the low dosage of PFA and the low starting water absorption in UHPC shorten the setting time. The entrained water released by PFA increases the spacing between cement particles and delay the bonding of the cementitious network.

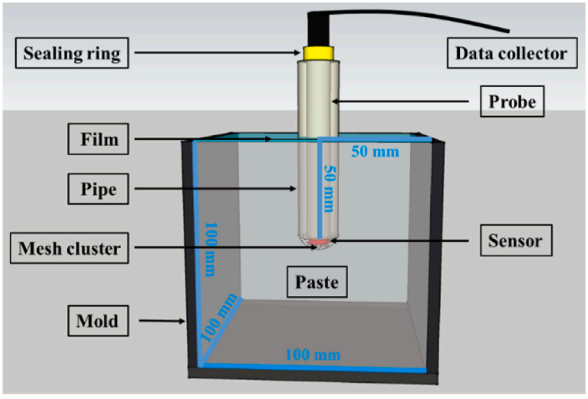

Fig. 6. 3D illustration of internal humidity and temperature fields monitoring device.

Table 5
Early age behaviors of the prepared UHPC slurry.

Num.	Fluidity (mm)	Setting time (min)	
		Initial	Final
C0	125	210	255
PFA_1C10	149	150	210
PFA_1C20	243	300	390
PFA_1C30	267	390	420
PFA_2C10	178	360	390
PFA_2C20	250	350	410
PFA_2C30	328	435	465
PFA_3C10	190	350	395
PFA_3C20	325	450	480
PFA_3C30	350	450	480

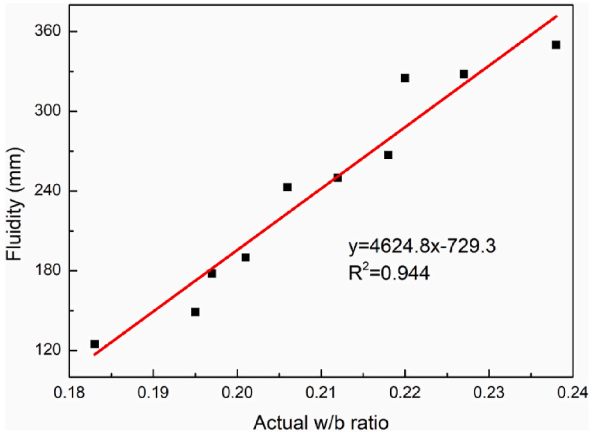

Fig. 7. Relationship between fluidity and actual w/b ratio of UHPC fresh mixtures prepared with PFA.

The formation of a hydrated shell layer around cement grains also affects the hardening of UHPC mortar [70]. Some detailed evidence and explanations for the differences in setting times of UHPC slurries containing PFA will be provided in Section 3.6 (hydration process evaluation).

3.2. Mechanical properties

The compressive strength development of UHPC prepared with various PFA contents and water adsorption is presented in Fig. 8. The compressive strength of samples made with higher proportions of PFA or higher water absorption is decreased at the early stages (1, 3 and 7 d). Higher proportions of wet PFA (e.g., PFA_1C10~C30) and higher water adsorption in the PFA (e.g., PFA_1~A_3) raise the

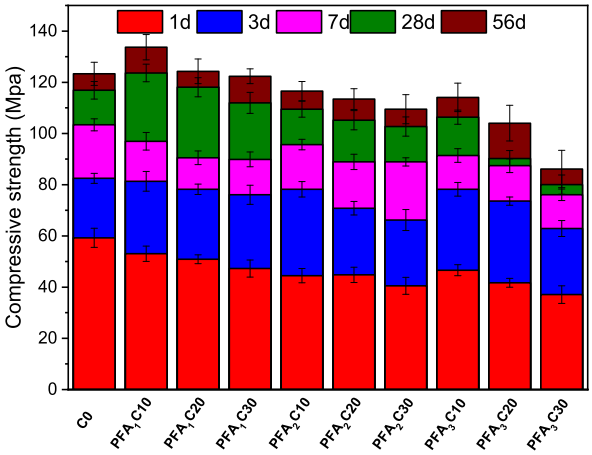

Fig. 8. Compressive strength development of UHPCs prepared with PFA.

actual w/b ratio in the mixture. The higher amount water also leads to a higher porosity as the voids left in the matrix after the hydration process, coherent with the lower mechanical strength of the UHPC mortars prepared with higher w/b ratio. Notably, more incorporated PFA also induce a higher porosity of the matrix and reduce the mechanical strength.

When PFA with a low water absorption rate is incorporated, a remarkable strength compensation enhancement can be observed in the later stages of UHPC, e.g., the 56 d compressive strength of PFA_1C10 is even higher than that of the reference group. As the compressive strength of C0 increases 19% from 7 d to 56 d, the compressive strength of PFA_1C10, PFA_1C20 and PFA_1C30 increased by 37%, 38% and 36%, respectively. This may be attributed to the water desorption of PFA, which promotes further hydration of the anhydrate cement particles in UHPC and secondary hydration of SF and FA [60]. It also enhances the gelation of the matrix and improves the interface transition zone [71].

Normally, the strength development of UHPC with PFA is related to the actual w/b ratio. But the pump effect of PFA shows its advantage in terms of water storage. For example, although the actual w/b ratio in PFA_1C10 (0.195) is higher than C0 (0.183), the later compressive strength of PFA_1C10 is higher than that of C0. Therefore, both the starting water absorption and PFA dosage play a significant role in the release of water. The PFA with a lower starting water absorption (PFA_1C10) has a stronger water retention capacity, limiting the water content released during the stirring process. The stored water would improve the hydration process in the longer stage.

3.3. Autogenous shrinkage evolution

Fig. 9 shows the evolution of autogenous shrinking of the UHPC mixtures prepared with various PFA contents and water adsorption. According to the previous studies, a typical evolution pattern of UHPC (e.g., PFA_1C10) can be divided into three stages [27,57], labeled as rapid shrinkage (**Stage I**), micro-expansion (**Stage II**) and continuous shrinkage (**Stage III**), respectively. **Stage I** lasts for about 0.5 d after "Time zero", whereas **Stage II** lasts for about 0.2 d. A remarkable distinction exists in the autogenous shrinkage evolution of the UHPC prepared with higher actual w/b ratios (PFA_1C30 and PFA_3C30). The autogenous shrinkage of the PFA_1C30 is almost negligible for the first 0.1 d and then enters a period of expansion lasting about 0.6 d. This remarkable pattern of evolution is defined as negligible deformation (**Stage O_1**) and sustained swelling (**Stage O_2**). Finally, a unified observation is found that the initiation time of **Stage III** is consistent in all UHPC groups, and that differences in the growth of shrinkage during this stage are limited in the PFA modified UHPC system. The autogenous shrinkage observed in this work for all types of mixtures is concluded in Fig. 9.

The occurrence of ***Stage O_1*** and ***Stage O_2*** reduces the overall volumetric deformation of the hardened UHPC when the pre-wetted PFA is incorporated, which has been widely observed in previous studies [52,53,58]. Furthermore, the thermal energy released by the hydration reaction of UHPC will form a temperature gradient distribution within the matrix, and thermal deformation will also play an essential role in the self-shrinkage behavior of UHPC. Compared with the reference group (C0), the 7 days autogenous shrinkage of PFA_2C30 and PFA_3C30 from **Stage O_1** was reduced by 34% and 48%, respectively. Moreover, PFA_1C30 exhibits a 60% decrease in total 7 days autogenous shrinkage starting from **Stage O_1** and **Stage O_2**. The gap between the total shrinkage of PFA_1C10 and C0 over 7 d narrows to 103%, a reflection of the IC effect of the wet PFA. Hence, the pre-wet PFA with abundant water entrainment has a significant shrinkage-reducing effect on UHPC. Furthermore, higher levels of PFA substitution with the same water adsorption can result in lower shrinkage for the UHPC matrix. Notably, the shrinkage reduction effect of the mixtures of PFA_3C20 and PFA_3C30 is remarkable (close to 50%). However, their 56 d compressive strengths are reduced by 15% and 30% respectively, which does not meet the strength requirements of the UHPC matrix. The IC design strategy of achieving shrinkage reduction by sacrificing mechanical properties is not desirable.

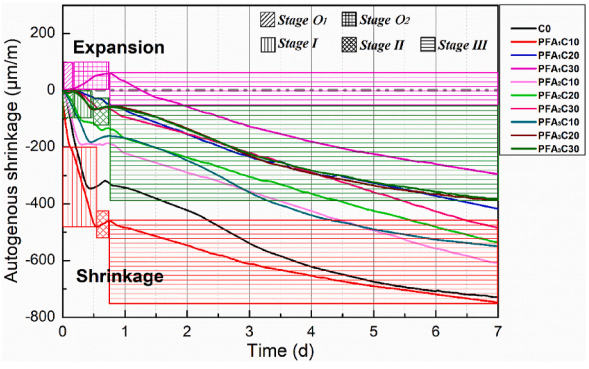

Annotation for breaking down autogenous shrinkage evolution curves:

1. *C0 and PFA_1C10 represents the mainstream evolution pattern;*
   Stage ***I***+Stage ***II***+Stage ***III***
2. *PFA_1C30 represents the special evolution pattern holding integral Stage **O**;*
   Stage ***O_1***+Stage ***O_2***+Stage ***III***
3. *PFA_3C30 represents the special evolution pattern merely possessing Stage ***O_1**;*
   Stage ***O_1***+ Stage ***I***+Stage ***II***+Stage ***III***

Fig. 9. Autogenous shrinkage behavior of UHPC prepared with PFA.

According to the obtained results, using pre-wet PFA with low water absorption and high replacement level (PFA_1C30) is an optimal strategy to design UHPC with advanced volumetric stability and mechanical properties. In terms of the actual w/b ratio, the obtained optimal result (0.218 in PFA_1C30) is consistent with the traditional *Powers* model of theoretical entrained water demand for IC [41] (Eq. (3)) (calculated value is 0.216). It is worth noting that if the total water/binder ratio is chosen to calculate the entrained water demand, the PFA_2C20 would be the optimal choice. Therefore, the theoretical entrained water demand for IC should be related to the maximum water desorption of PFA and should be calculated with the actual water/binder ratio rather than the total water/-binder ratio. This work evidences the feasibility of the *Powers* model in the designed UHPC prepared with PFA, and the water desorption behavior of PFA should be considered when the *Powers* model is applied.

$$(w/b)_{IC} = \begin{cases} 0.18 \times (w/b) & (w/b) \le 0.36 \\ 0.42 - (w/b) & 0.36 < (w/b) \le 0.42 \end{cases} \tag{3}$$

However, the autogenous shrinkage behavior of the PFA-containing UHPC is not ordered by its entrained water demand, indicating a more complicated interaction when PFA is incorporated into the UHPC. The *Powers* model is based on the phase distribution of the cementitious materials and does not consider the potential influence of the water adsorption-desorption behavior of the porous IC agents on the physical and chemical properties of the mortar. Therefore, it is not sufficient to rely solely on *Powers* model to reveal the multi-stage evolution of the autogenous shrinkage development of UHPC when porous IC agents are added. To investigate the multiple intrinsic mechanisms of the autogenous shrinkage evolution of UHPC with PFA and their potential driving force, the hydration behavior, internal humidity and temperature fields of some selected mixtures were further characterized and explained.

3.4. Phases assemblage in UHPC for stage O_1

As pointed out in section 3.3, the potential expansion can significantly mitigate the total autogenous shrinking deformation of UHPC prepared with PFA. Generally, the expansion in cementitious materials can be attributed to the formation of expansive hydration products, such as aluminum ferrite trisubstituted (AFt) needles, aluminate ferrite monosubstituted (AFm) crystals, portlandite (CH) and C–S–H gels [57,72–75]. In order to clarify the potential reasons for the expansion, PFA_1C30, PFA_2C30 and PFA_3C30 were investigated.

Fig. 10 shows the XRD patterns of the selected samples and the raw materials. The specific peaks of brownmillerite (C_4AF) from the OPC 52.5 are still present in the XRD patterns of all mixtures, indicating a low hydration degree of UHPC within 5 h. Besides, the peak (9.12°, 2θ) of ettringite is invisible in all tested groups. The formation of ettringite is limited in UHPC at an early age, which is coherent with the results previous reported by Korpa et al. [76]. The relatively low w/b ratio and slow dissolution rate of the aluminate in UHPC hinder the formation of ettringite at an early stage.

Fig. 11 presents the DTG curves of the selected samples and raw PFA. Since no other bound water contained minerals found in the XRD analysis, the weight loss in interval **I** is mainly attributed to dehydration of the C–S–H gel [67]. The mass loss around interval **II** is assigned as the dehydration of portlandite. In interval **III** (500–800 °C), the peaks of PFA_1C30, PFA_2C30 and PFA_3C30 are associated with the decarbonation of PFA (the main component is calcite). Only minor differences are visible on the interval **I** (40–200 °C) and **II** (400–500 °C), indicating a similar formation content of those minerals. Herein, the potential expansion in UHPC prepared with PFA at an early age cannot be attributed to the CH and C–S–H. Furthermore, the formation of CH and C–S–H amplifies the chemical shrinkage of UHPC.

As mentioned above, limited additional expansive hydration products were found in the hardened UHPC with PFA. Therefore, the additional formation of expansive hydration products is not suitable to explain the existence of **Stage O_1** for UHPC prepared with PFA. Notably, **Stage O_1** only exists in the group of UHPC prepared with a high actual w/b ratio, which can be ascribed to an extra liquid volume compensation effect. A schematic diagram relating to these explanations is illustrated in Fig. 12. The release of water (that

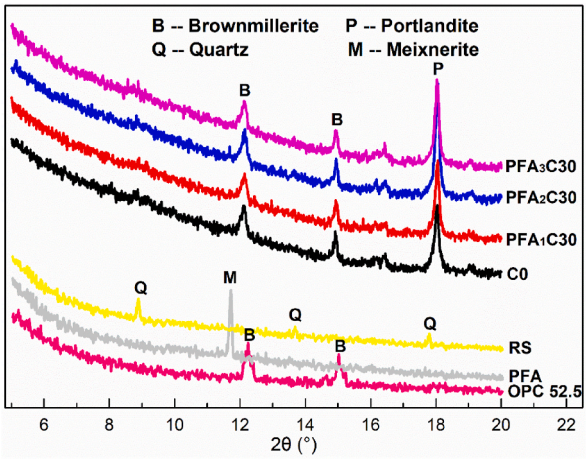

Fig. 10. XRD patterns of the investigated UHPC hardened pastes at 5 h old.

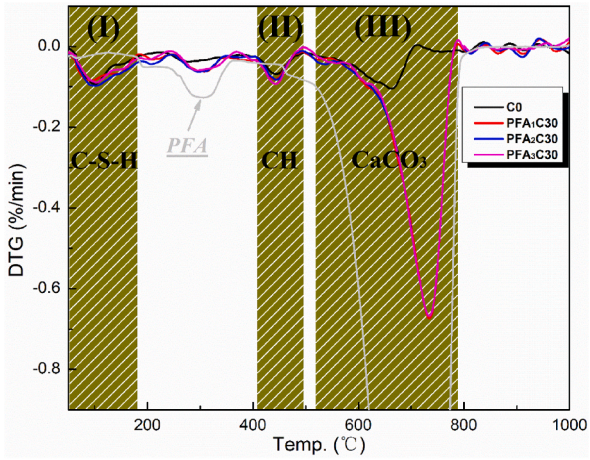

Fig. 11. DTG spectrum of the investigated UHPC hardened pastes at 5 h after final setting point.

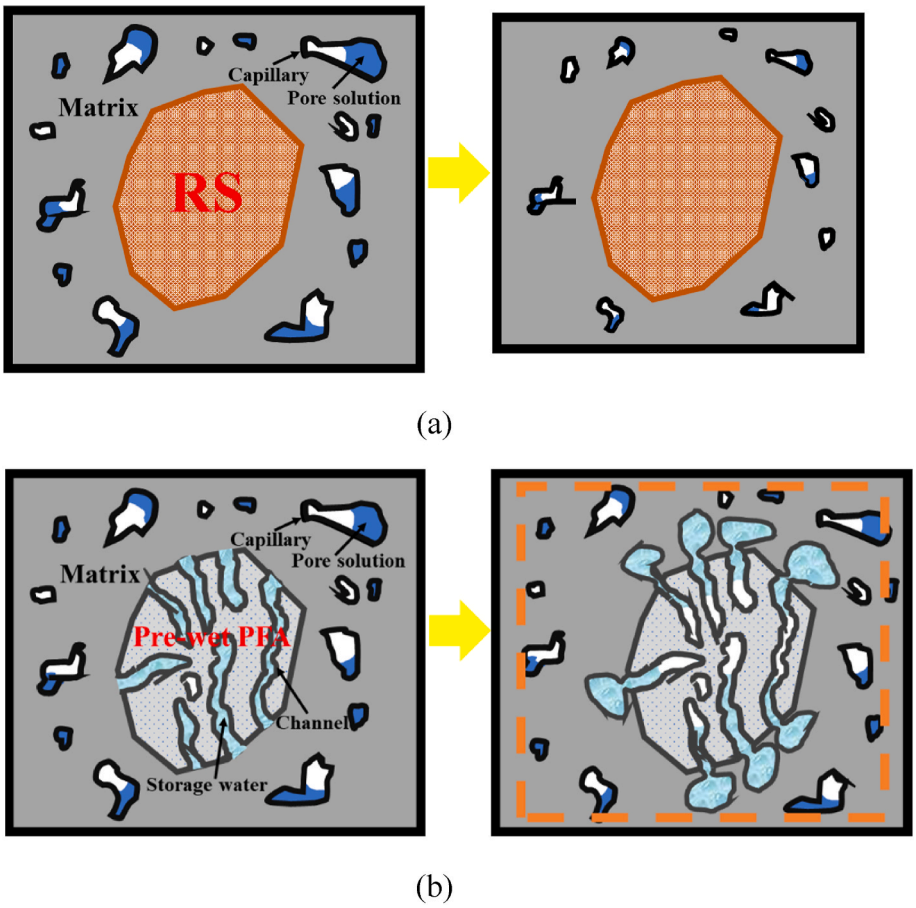

Fig. 12. Deformation behavior of UHPC hardened paste under the effect of moisture released from PFA: UHPC prepared with (a) RS, (b) PFA_1.

stored in PFA channels without volume contribution) from PFA increases the total volume of the mortar, offsetting most of the shrinkage caused by hydration. In addition, the reabsorption of bleeding water after the setting may also result in an expansion at early age, as reported elsewhere [77].

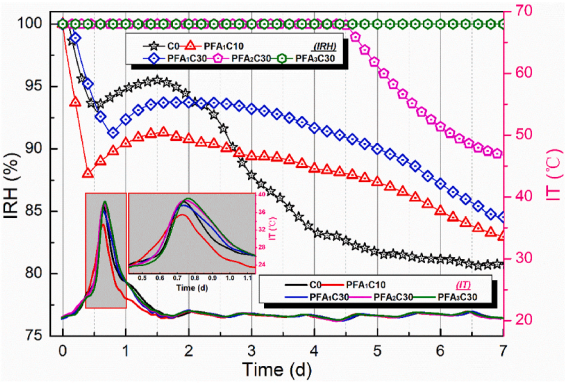

Annotation for breaking down IRH evolution curves:
*C0 and PFA$_1$C30: Phase **i**+ Phase **ii**+ Phase **iii** +Phase **iv***
*PFA$_1$C10: Phase **ii**+ Phase **iii** +Phase **iv***
*PFA$_2$C30: Phase **i**+ Phase **iv***
*PFA$_3$C30: Phase **i***

Fig. 13. IRH and IT evolution inside several representative UHPC specimens mixing with pre-soaked PFA during the first week after the final setting point.

3.5. Internal humidity and temperature evolution for stage O_2 and II

Fig. 13 shows the evolution of IRH and internal temperature (IT) for the first 7days for several representative samples. It can be seen that the IRH shows different evolutionary trends among the different UHPC mixtures, as concluded in the annotation. The evolution of the PFA modified UHPC with low water adsorption (PFA$_1$) is defined as four-phase, i.e., temporary stability with 100% IRH (**Phase i**), cliff-like descent (**Phase ii**), rebound (**Phase iii**) and sustained decline (**Phase iv**). The UHPC prepared with the higher water adsorption PFA$_2$ and PFA$_3$ can remain saturated for a long period (IRH = 100%) and a significant drop in IRH takes a few days. In terms of IT, a 1.5-days long zone of concentrated heating occurs (also observed in Refs. [10,61]). The peak appears approximately 0.75 days with a temperature rise of 15–20 °C.

The evolution of IRH in the UHPC is sensitive to the starting water absorption of the incorporated PFA. Table 6 summarizes the duration and contribution of each phase in the evolution of IRH for the samples incorporated with low water adsorption PFA (C0, PFA$_1$C10, PFA$_1$C30). It can be seen that the differences between the occurrence and duration of **Phase i** and **ii** in PFA$_1$C10 and PFA$_1$C30 compared with that in C0 are consistent with the regularity of their setting time. The IRH values of PFA$_1$C10 and PFA$_1$C30 are lower at the end of **Phase ii** than in C0, which is related to the pumping effect of PFA$_1$. The IRH values for C0, PFA$_1$C10 and PFA$_1$C30 then rebounded at **Phase iii** (also observed in Ref. [60]). It is noteworthy that in all tested groups, the highest points in **Stage II** (in C0, PFA$_1$C10, PFA$_2$C30 and PFA$_3$C30) and **Stage O_2** (in PFA$_1$C30) strictly overlap with the peaks of IT, indicating that thermal expansion is exactly the main driver of the autogenous shrinkage behavior of their specimens during this stage. The rise of IT, caused by the released heat by hydration, leads to the expansion of the moisture, followed by a decrease in the surface tension of water in the capillary. Enhancing the radius of curvature of the meniscus liquid surface and the pore fluid pressure leads to a rebound in IRH [78], as illustrated in Fig. 14(a). There is a lag of approximately 0.75 days in the arrival of the IRH peak in **Phase iii** compared with the maximum IT time. This may be attributed to the different thermal expansion coefficients of the matrix and moisture, as the cold contraction of the matrix squeezes the liquid surface in the capillaries, resulting in a continuous rise in IRH, as shown in Fig. 14(b). In **Phase iv**, the rate of IRH decline for PFA$_1$C10 and PFA$_1$C30 is significantly slower compared to C0 due to the compensation of IRH by wet PFA. Fig. 15 reveals the relationships between the development of autogenous shrinkage (AS) and the rate of IRH (ΔIRH) decline in C0, PFA$_1$C10 and PFA$_1$C30, where the parabolic equations are matched in **Phase iv**. Therefore, the capillary pressure is the main force behind the shrinkage of UHPC at **Phase iv**.

On the other hand, the samples prepared with PFA containing higher water adsorption (PFA$_2$C30 and PFA$_3$C30) maintain 100%

Table 6
Duration and contribution of each phase in IRH evolution process of UHPC specimens mixing with water-deficient PFA and without IC agent.

Multi-phases		C0	PFA$_1$C10	PFA$_1$C30
Phase i (Temporary stability)	Duration	2.5 h	0	3.5 h
	Contribution	0	0	0
Phase ii (Cliff-like descent)	Duration	11 h	9.5 h	15.5 h
	Contribution	−7%	−12%	−9%
Phase iii (Rebound)	Duration	23 h	29 h	36 h
	Contribution	+2.5%	+3.3%	+2.4%
Phase iv (Sustained decline)	Duration	131.5 h	129.5 h	113 h
	Contribution	−14.8%	−8.3%	−9.2%

"-" indicates the decrease of IRH, "+" indicates the increase of IRH.

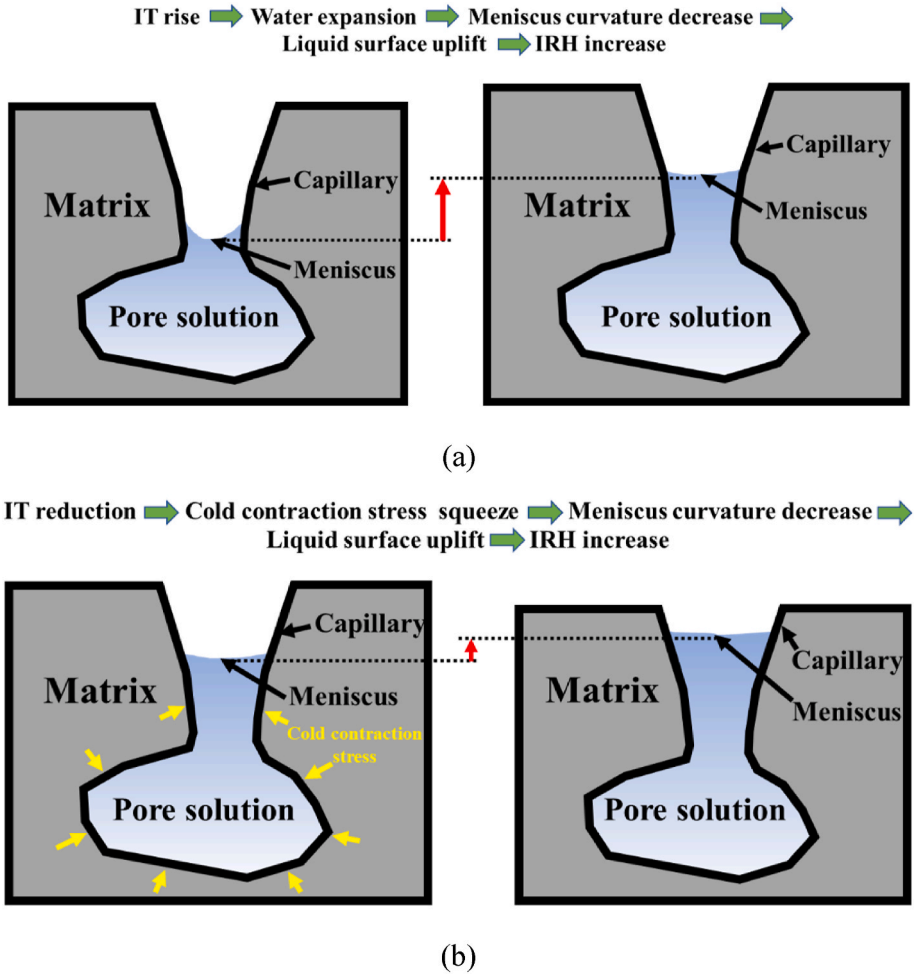

Fig. 14. Variations of meniscus liquid surface curvature in capillary pore and matrix IRH (caused by IT evolution inside UHPC): (a) heating period, (b) cooling period (modified from Ref. [78]).

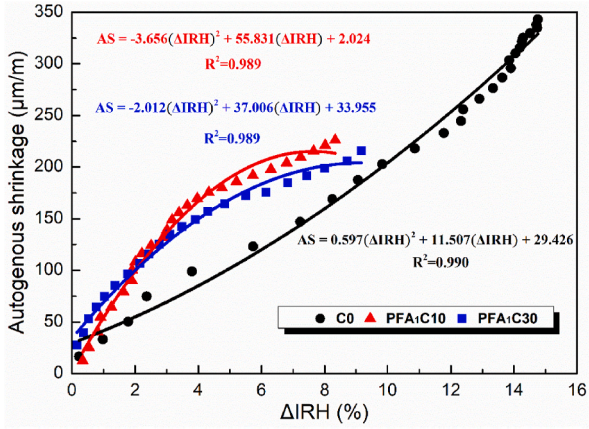

Fig. 15. Relationships between the development of autogenous shrinkage and the drop rate of IRH in UHPC combined with thirsty PFA or without IC during **Phase iv**.

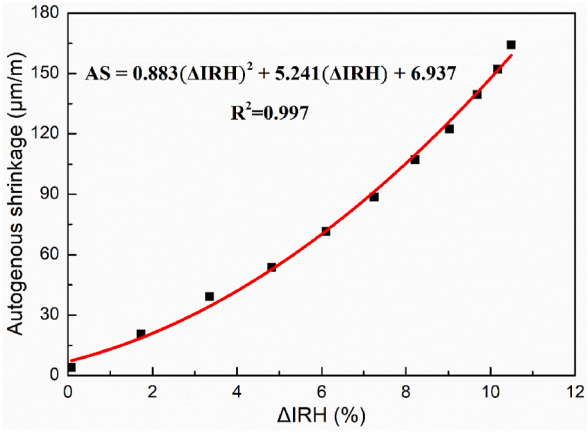

Fig. 16. Correlation of autogenous shrinkage (AS) and IRH drop rate (ΔIRH) in PFA_2C30 during IRH descent period (from 4.5 d up to 7 d).

IRH for approximately 4.5 days and 7 days or more, respectively. The same observations have been demonstrated by other researchers [43,57,59,60]. The continuous release of water from PFA maintains a saturation state of IRH inside UHPC. As seen in Fig. 9, PFA_2C30 and PFA_3C30 show similar development of autogenous shrinkage up to 4.5 d. The autogenous shrinkage of PFA_2C30 then accelerates after 4.5 d, which is coherent with the decrease in IRH values in Fig. 13. Fig. 16 shows the relationship between the development of autogenous shrinkage (AS) of PFA_2C30 from 4.5 d to 7 d and the rate of decrease in IRH (ΔIRH). Thus, when higher water adsorption PFA_2 is used in the UHPC, the autogenous shrinkage of the matrix is also driven by the capillary pressure at later **Stage III**, but is dominated by chemical and cold shrinkage at early **Stage III** (when IRH is maintained at 100%).

3.6. *Hydration process evaluation for stages I and III*

Fig. 17 shows the heat flow and accumulated heat of hydration for the selected recipes of UHPC within the first 7 days. As shown in Fig. 17(a), the main exothermic peak of all mixtures exists around 0.5 d, which is attributed to the formation of massive hydration products. However, the hydration process is delayed in the UHPC prepared with PFA. The entrained water from PFA leads to a higher actual w/b ratio and increases the induction period. A layer of hydration products covers the individual cement particles and retards further hydration process [70], which is consistent with the delayed setting time in Section 3.1. In Fig. 17(b), the released heat increases rapidly in the first 0.75 d, consistent with the evolution of IT described in Section 3.5. The tiny temperature difference in the evolution of IT is considered to be related to the development of matrix microstructure [10,60,61]. The free water released from PFA can eventually participate in the hydration process, promoting the accumulative heat and enhancing the hydration degree of cement particles at a longer stage. This finding also coincides with the later mechanical strength compensation, as shown in Fig. 8.

Additionally, the degree of hydration in UHPC over time can be estimated according to the following equation (Eq. (4)) [79]:

$$\alpha = \frac{Q_{(t)}}{Q_{pot}} \tag{4}$$

where α, $Q_{(t)}$ and Q_{pot} denote the degree of hydration at a particular time (%), the cumulative heat released at the point in the hydration process (J/g) and the potential hydration heat for complete hydration of the binder (J/g), respectively. The primary raw materials in the UHPC mixtures are evaluated to calculate the Q_{pot} value. FA is involved in hydration very late (after 28 d) and its heat of hydration reaction is extremely low and negligible compared to that of cement [80–82]. The chemical composition of OPC 52.5 is then used to determine the content of the four major mineral phases in the clinker. The heat released by each phase in the clinker is quoted from the literature [79] and is detailed in Table 7. In addition, SF has a low reactivity and acts mainly as a filler in UHPC, with a reported reactivity of about 15% in mature UHPC [83]. The dissolution and the pozzolanic reaction of SF (mainly amorphous SiO_2) follow the equation (Eq. (5)) with an enthalpy change (ΔH) of +863 J/g for the reaction [84,85].

$$SiO_2\ (am) + 0.65\ Ca(OH)_2 + 0.85H_2O = (CaO)_{0.65}(SiO_2)\ (H_2O)_{1.5} \tag{5}$$

Finally, the Q_{pot} value is calculated based on the clinker and SF content of the test mixture and the hydration degree at a particular time is estimated.

Based on the calculation criteria mentioned above, the relationship between instantaneous hydration degree and actual w/b ratio in the investigated UHPC mixture at 12 h, 24 h, 48 h and 168 h is plotted in Fig. 18. As we can see, the various water adsorption of PFA in the UHPC leads to the different actual w/b ratios, with the hydration degree of each mixture varying by reaction time. After 24 h, the hydration degree is positively correlated with the actual w/b ratios, which is consistent with the ending time of the main hydration exothermic peak.

The autogenous shrinking behavior of the matrix is mainly influenced by the hydration of cementitious materials, and several studies have reported that the hydration degree correlates with the development of autogenous shrinkage [5,86–88]. Fig. 19 reveals the hydration degree development of the selected UHPC mixture within 7 days. At **Stage I**, the autogenous shrinkage behavior of C0,

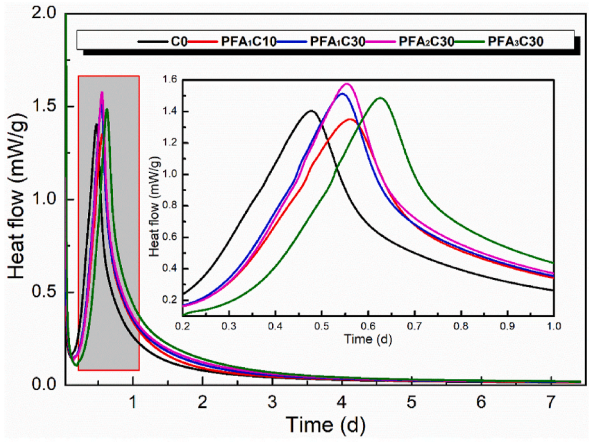

(a)

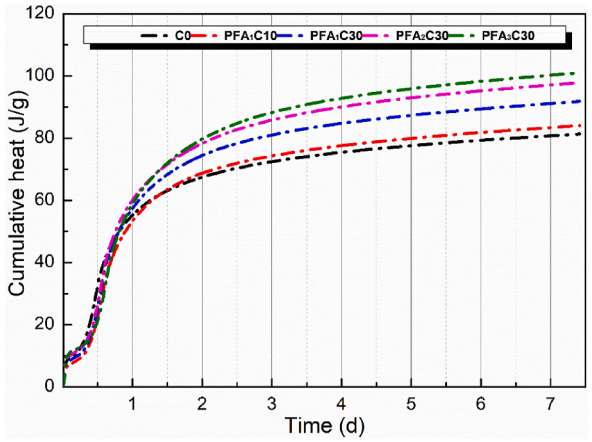

(b)

Fig. 17. Hydration heat flow and accumulative heat of the representative UHPC during the first 7 days: (a) heat flow; (b) accumulative heat.

Table 7
Calculation parameters of released heat for the mineral phases.

Clinker phase	C_3S	C_2S	C_4AF	C_3A
Percentage (wt. %)	63.84	12.04	9.87	6.64
Released heat (J/g)[a]	500	250	420	1340

[a] Cited from [79].

PFA_1C10, PFA_2C30 and PFA_3C30 fits the hydration degree development, as illustrated in Fig. 20. The excellent fit coefficients indicate that at **Stage I**, the rapid growth of shrinkage deformation is caused by the hydration dynamic involved in several changes such as IRH, IT, and phase transformation. The hydration dynamics are the dominant driving force at **Stage I**. As pointed out in section 3.5, **Stage III** starts with a cold shrinkage of the matrix of 0.8 d. The IRH and IT values remain stable for PFA_1C30 (from 1.5 to 2.3 days), PFA_2C30 (from 1.5 to 4.5 days) and PFA_3C30 (from 1.5 to 7 days). The relationship between the autogenous shrinkage and the hydration degree during this period is shown in Fig. 21. It confirms that the chemical shrinkage is the major driver of autogenous shrinkage during this stage.

3.7. Summaries of the multiple mechanisms and driving forces

The autogenous shrinking of UHPC prepared with pre-wetted PFA is affected by multiple factors such as the water content and desorption behavior of PFA as well as the IRH gradient, the hydration process, and the thermal deformation of the UHPC matrix. In detail, the driving force of **Stage O_1** is the bulk compensation of the PFA desorption water, as explained in Section 3.4. **Stage O_2** is considered to be driven by the thermal expansion caused by the hydration heat outweighing the sum of the extra chemical shrinkage

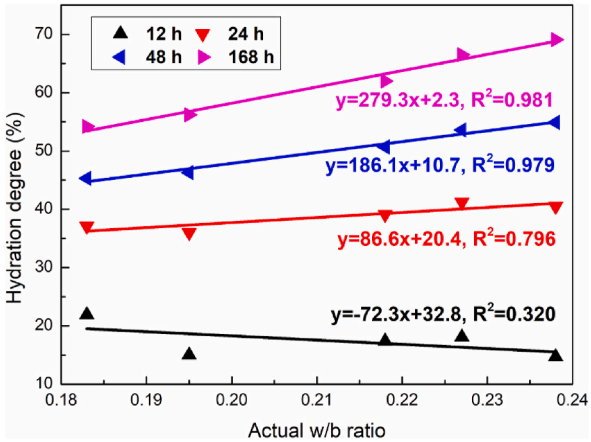

Fig. 18. Relationships between instant hydration degree (at 12 h, 24 h, 48 h and 168 h) and actual w/b ratio (C0, PFA_1C10, PFA_1C30, PFA_2C30 and PFA_3C30).

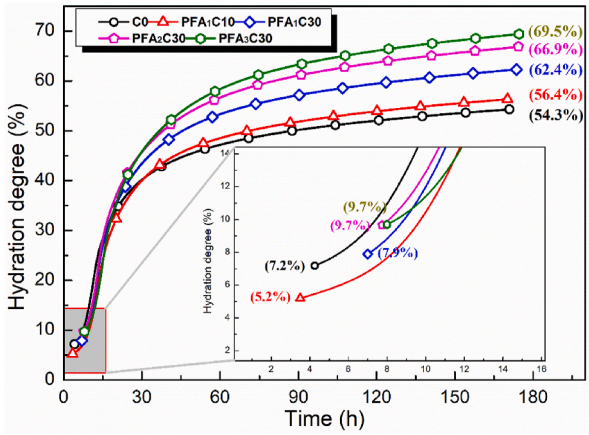

Fig. 19. Hydration degree of the studied UHPC groups within one week after the final setting point (C0, PFA_1C10, PFA_1C30, PFA_2C30 and PFA_3C30).

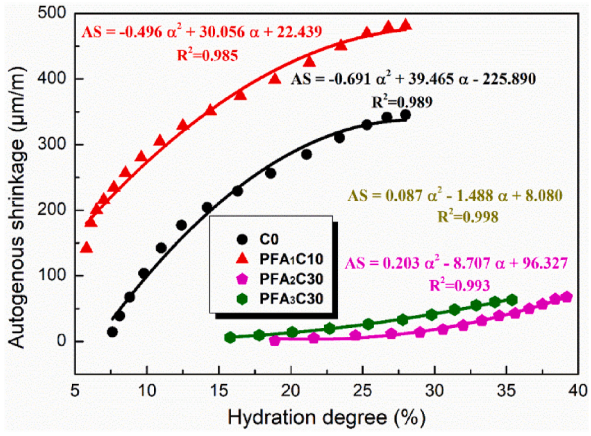

Fig. 20. Correlations of autogenous shrinkage (AS) and hydration degree (α).
at Stage I (C0, PFA_1C10, PFA_2C30 and PFA_3C30).

and self-shrinkage. Furthermore, **Stage O_2** does not occur in the group where excess water is introduced, which is also related to the weaker gel strength reducing its constraint on matrix shrinkage [61,89]. In **Stage I** of C0 and PFA_1C10, the increased shrinkage induced by IRH cliff fall (**Phase ii**) overwhelms the thermal expansion; in PFA_2C30 and PFA_3C30, the extra chemical shrinkage plays a

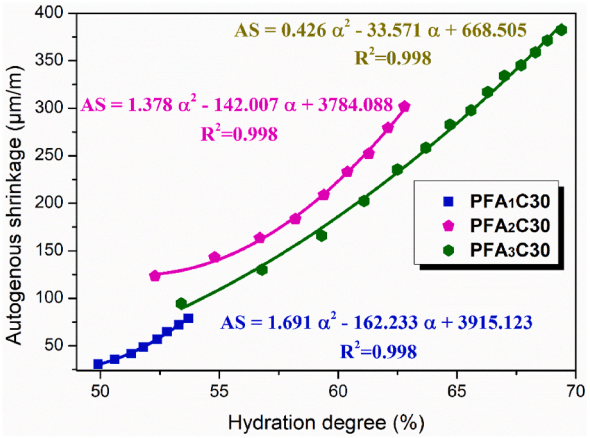

Fig. 21. Correlations of autogenous shrinkage (AS) and hydration degree (α) during the verified **Stage III** without IRH and IT interference (PFA_1C30, PFA_2C30 and PFA_3C30).

dominant role in the thermal expansion [90]. **Stage II** is identified as the effect of IT, with thermal dilation greater than all types of shrinkage. **Stage III** begins with a 0.8 d cold shrinkage of the matrix [91], accompanied by an IRH drop. When IT returns to the ambient as a period of monotonically declining IRH, a binomial correlation between the development of autogenous shrinkage and ΔIRH in UHPC is elaborated. Then the capillary pressure is the dominant driver of the autogenous shrinkage.

Based on the above results and discussion, Fig. 22 summarizes the main influencing mechanisms and driving forces for the different stages of autogenous shrinkage evolution for UHPC incorporating PFA as IC agent. The autogenous shrinkage evolution of UHPC (with pre-wetted PFA) is governed by a combination of various physical (liquid volume compensation, thermal expansion, cold shrinkage and capillary pressure) and chemical (hydration dynamic and chemical shrinkage) effects. Specifically, the rapid shrinkage growth stage (**Stage I**) of the UHPC matrix is managed by hydration dynamics (indicated by the hydration degree). The micro-expansion (**Stage II**) is caused by thermal expansion. The continued shrinkage (**Stage III**) is managed by cold shrinkage, chemical shrinkage and capillary pressure.

When the chemical reaction is dominant, the development of autogenous shrinkage of the UHPC matrix is related to its hydration degree. During the regulated period when capillary pressure dominates, the development of autogenous shrinkage of the UHPC matrix is similarly correlated with a decline of IRH. In the case of sufficient IC, a short, negligible deformation stage (**Stage O_1**) occurs at the super early hardening of UHPC mortar due to the compensating effect of extra liquid volume of entrained water. If the PFA has a high water retention capacity, then a sustained expansion stage (**Stage O_2**) of matrix deformation will follow, bringing the best shrinkage reduction for UHPC. Otherwise, the matrix deformation of UHPC will follow the typical shrinkage pattern.

In general, the unique stage (**Stage O** or **II**) in the evolution of autogenous shrinkage of UHPC incorporating pre-wetted PFA, especially **Stage O**, is quite beneficial to improve the volumetric stability of the UHPC matrix. Furthermore, as a fundamental requirement for UHPC, the mechanical properties are sensitive to the actual w/b ratio of the gelling system. It should not be neglected when designing the water entrainment demand of ICs. In this work, the evolution of autogenous shrinkage demonstrates the applicability of the *Powers* model in the design of UHPC prepared with pre-wetted PFA. However, the desorption behavior of PFA should be taken into account when calculating the entrained water of ICs, which has significant implications for the actual water/binder ratio in the mixture. According to the investigations shown in this study, the deformation of the hardened matrix within 0.75 days is the most critical for the final shrinkage, which is also the crucial period for IC conditioning. Therefore, a relatively high PFA content and moderate water absorption (non-saturated state) as IC medium should be the best strategy to produce UHPC with advanced volumetric stability.

4. Conclusions

In this study, the PFA with different water adsorption and dosages were applied in the UHPC and its autogenous shrinkage was investigated. The main driving mechanisms for the evolution of the autogenous shrinkage of UHPC (with/without PFA) at different periods/stages were analyzed and discussed. Based on the obtained results, the major conclusions can be summarized as follows:

(1) The evolution of autogenous shrinkage of UHPC (with or without PFA) can be divided into multi-stages. Pre-wetted PFA remarkably reduces the autogenous shrinkage deformation of UHPC by up to 60% within 7 days. The water desorption of PFA also leads to a longer setting time, but with better volumetric stability.
(2) The evolution of autogenous shrinkage of UHPC (with pre-wet PFA) is governed by a combination of physical (liquid volume compensation, thermal expansion, cold shrinkage and capillary pressure) and chemical (hydration dynamic and chemical shrinkage) effects.
(3) IRH in UHPC with unsaturated PFA undergoes four phases: temporary stability, cliff-like descent, rebound and sustained decline. Furthermore, IRH in UHPC with water-rich PFA remains saturated for a few days and continued to decline remarkably.

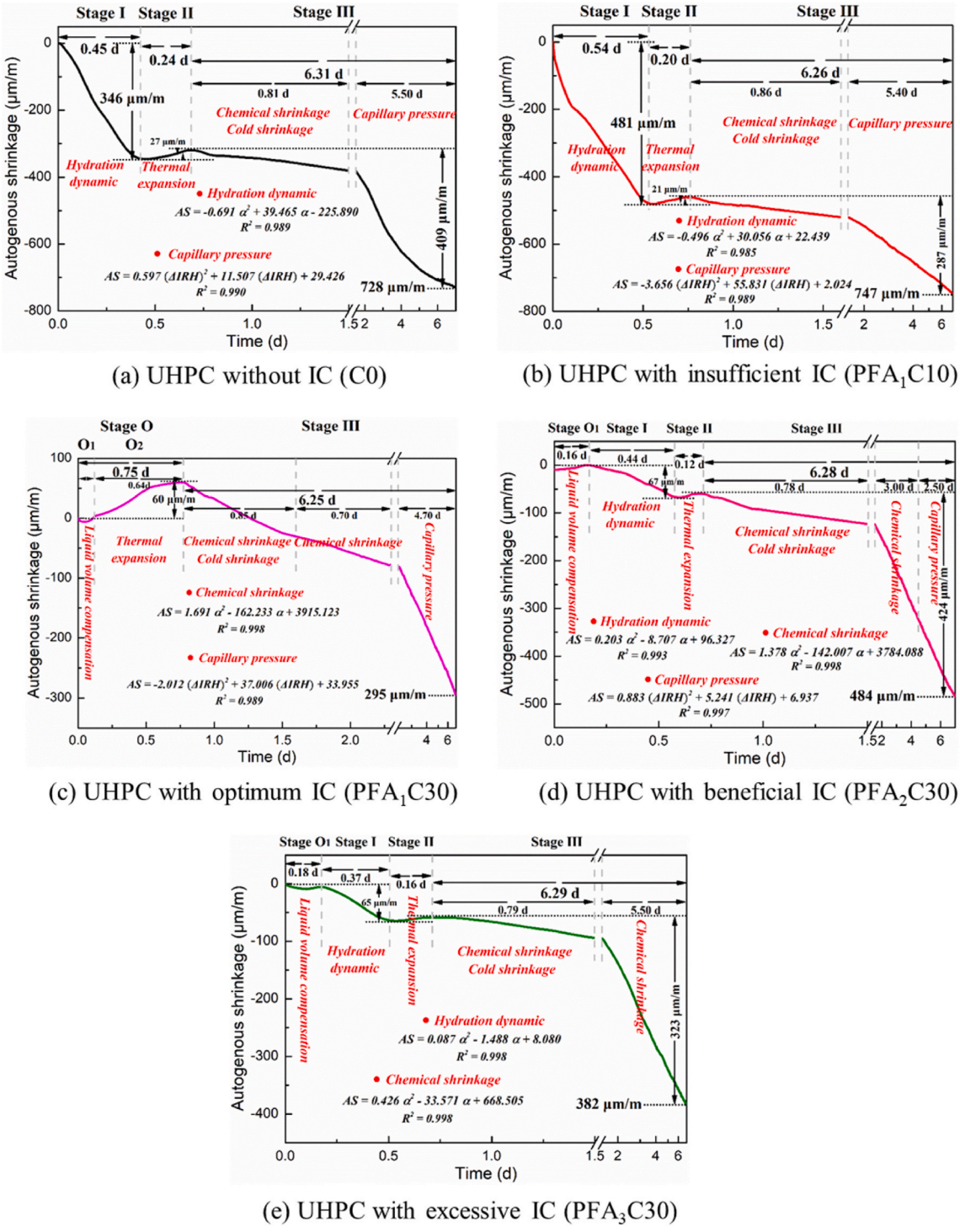

Fig. 22. Main influencing mechanisms and driving forces for the different stages of the autogenous shrinkage evolution in UHPC incorporating PFA IC agent.

During the continuous decline phase of IRH, the autogenous shrinkage of UHPC develops relative to the drop rate of IRH. In addition, thermal deformation and the IRH rebound are attributed to a concentrated heating zone with a maximum temperature rise of 15–20 °C within 1.5 days inside the hardened UHPC.

(4) The potential expansion driving force of UHPC at the super early hardening period should not be attributed to the formation of expansive hydration products, but rather to the effect of extra liquid volume compensation and thermal expansion.

(5) The rapid shrinkage stage of UHPC is multiply affected by self-shrinkage, thermal deformation and chemical shrinkage. Moreover, the development of autogenous shrinkage development of UHPC can correlate with its hydration degree. Meanwhile, during the continuous shrinkage stage, the interval before IRH and IT decline is dominated by chemical shrinkage.
(6) Based on the findings of the autogenous shrinkage evolution drivers, the conventional Powers model is still applicable for the design of water demand in the porous IC medium incorporated in UHPC. The desorption behavior of PFA should be considered and the actual water/binder ratio should be calculated as the optimal entrained water content in ICs. In this study, it has been demonstrated that a relatively high PFA content with moderate water absorption (non-saturated state) is the best combination for producing UHPC with advanced volumetric stability.

CRediT authorship contribution statement

Kaizhi Liu: Conceptualization, Methodology, Investigation, Data curation, Formal analysis, Validation, Writing – original draft. **Yong Long:** Investigation, Supervision. **Luyi Chen:** Investigation, Supervision. **Xuan Ling:** Writing – review & editing, Conceptualization, Formal analysis. **Rui Yu:** Supervision, Writing – review & editing. **Zhonghe Shui:** Supervision, Writing – review & editing, Funding acquisition. **Shunxin Fei:** Investigation. **Wenzhi Yu:** Investigation. **Chen Li:** Investigation. **Keyu Ge:** Investigation.

Declaration of competing interest

The authors declare that they have no known competing financial interests or personal relationships that could have appeared to influence the work reported in this paper.

Acknowledgements

The authors would like to acknowledge the financial supports of National Nature Science Foundation Project of China (51608409, 51679179), Key Research Project of China Railway Major Bridge Engineering Group Co., Ltd (2021-44-Key), Open Projects Foundation of State Key Laboratory for Health and Safety of Bridge Structures (BHSKL21-08-KF) and the funding of China Scholarship Council (No. 201906950015).

References

[1] P. Richard, M. Cheyrezy, Composition of reactive powder concretes, Cement Concr. Res. 25 (7) (1995) 1501–1511.
[2] C. Shi, Z. Wu, J. Xiao, D. Wang, Z. Huang, Z. Fang, A review on ultra high performance concrete: Part I. Raw materials and mixture design, Construct. Build. Mater. 101 (2015) 741–751.
[3] D. Wang, C. Shi, Z. Wu, J. Xiao, Z. Huang, Z. Fang, A review on ultra high performance concrete: Part II. Hydration, microstructure and properties, Construct. Build. Mater. 96 (2015) 368–377.
[4] J. Du, W. Meng, K.H. Khayat, Y. Bao, P. Guo, Z. Lyu, A.O. Adi, H. Nassif, H. Wang, New development of ultra-high-performance concrete (UHPC), Compos. B Eng. 224 (9) (2021) 109220.
[5] P. Lura, O.M. Jensen, K.V. Breugel, Autogenous shrinkage in high-performance cement paste: an evaluation of basic mechanisms, Cement Concr. Res. 33 (2003) 223–232.
[6] M. Zhang, C.T. Tam, M.P. Leow, Effect of water-to-cementitious materials ratio and silica fume on the autogenous shrinkage of concrete, Cement Concr. Res. 33 (10) (2003) 1687–1694.
[7] K. Koh, G. Ryu, S. Kang, J. Park, S. Kim, Shrinkage properties of ultra-high performance concrete (UHPC), Adv. Sci. Lett. 4 (3) (2011) 948–952.
[8] A.M. Soliman, M.L. Nehdi, Effect of drying conditions on autogenous shrinkage in ultra-high performance concrete at early-age, Mater. Struct. 44 (2011) 879–899.
[9] V.Y. Garas, L.F. Kahn, K.E. Kurtis, Short-term tensile creep and shrinkage of ultra-high performance concrete, Cement Concr. Compos. 31 (3) (2009) 147–152.
[10] T. Xie, C. Fang, M.S.M. Ali, P. Visintin, Characterizations of autogenous and drying shrinkage of ultra-high performance concrete (UHPC): an experimental study, Cement Concr. Compos. 91 (2018) 156–173.
[11] Y. Bao, W. Meng, Y. Chen, G. Chen, K.H. Khayat, Measuring mortar shrinkage and cracking by pulse pre-pump Brillouin optical time domain analysis with a single optical fiber, Mater. Lett. 145 (2015) 344–346.
[12] Z.P. Bažant, S. Baweja, Creep and shrinkage prediction model for analysis and design of concrete structures: Model B3, Mater. Struct. 28 (1995) 357–365.
[13] D. Hou, W. Zhang, M. Sun, P. Wang, M. Wang, J. Zhang, Z. Li, Modified Lucas-Washburn function of capillary transport in the calcium silicate hydrate gel pore: a coarse-grained molecular dynamics study, Cement Concr. Res. 136 (2020) 106166.
[14] E. Holt, Contribution of mixture design to chemical and autogenous shrinkage of concrete at early ages, Cement Concr. Res. 35 (3) (2005) 464–472.
[15] Z. Jiang, Z. Sun, P. Wang, Internal relative humidity distribution in high-performance cement paste due to moisture diffusion and self-desiccation, Cement Concr. Res. 36 (2006) 320–325.
[16] J. Zhang, D. Hou, Y. Han, Micromechanical modeling on autogenous and drying shrinkages of concrete, Construct. Build. Mater. 29 (2012) 230–240.
[17] O.M. Jensen, P.F. Hansen, Autogenous deformation and RH-change in perspective, Cement Concr. Res. 31 (12) (2001) 1859–1865.
[18] O.M. Jensen, Thermodynamic limitation of self-desiccation, Cem. Concr. Res. 25 (1) (1995) 157–164.
[19] C.F. Ferraris, F.H. Wittmann, Shrinkage mechanisms of hardened cement paste, Cement Concr. Res. 17 (3) (1987) 453–464.
[20] C. Hua, P. Acker, A. Ehrlacher, Analyses and models of the autogenous shrinkage of hardening cement paste. I. Modelling at macroscopic scale, Cement Concr. Res. 25 (7) (1995) 1457–1468.
[21] S. Diamond, Mercury porosimetry: an inappropriate method for the measurement of pore size distributions in cement-based materials, Cement Concr. Res. 30 (10) (2000) 1517–1525.
[22] L.R. Fisher, J.N. Israelachvili, Experimental studies on the applicability of the Kelvin equation to highly curved concave menisci, J. Colloid Interface Sci. 80 (2) (1981) 528–541.
[23] D.P. Bentz, E.J. Garboczi, D.A. Quenard, Modelling drying shrinkage in reconstructed porous materials: application to porous Vycor glass, Model. Simulat. Mater. Sci. Eng. 6 (1998) 211–236.
[24] H. Ye, A. Radlińska, A review and comparative study of existing shrinkage prediction models for portland and non-portland cementitious materials, Adv. Mater. Sci. Eng. (2016) 2418219.
[25] Y. Li, J. Li, Capillary tension theory for prediction of early autogenous shrinkage of self-consolidating concrete, Construct. Build. Mater. 53 (2014) 511–516.
[26] A.M. Soliman, M.L. Nehdi, Effects of shrinkage reducing admixture and wollastonite microfiber on early-age behavior of ultra-high performance concrete, Cement Concr. Compos. 46 (2014) 81–89.

[27] D.Y. Yoo, N. Banthia, Y.S. Yoon, Effectiveness of shrinkage-reducing admixture in reducing autogenous shrinkage stress of ultra-high-performance fiber-reinforced concrete, Cement Concr. Compos. 64 (2015) 27–36.
[28] L. Yang, C. Shi, Z. Wu, Mitigation techniques for autogenous shrinkage of ultra-high-performance concrete - a review, Compos. B Eng. 178 (1) (2019) 107456.
[29] S.H. Park, G.S. Ryu, K.T. Koh, D.J. Kim, Effect of shrinkage reducing agent on pullout resistance of high-strength steel fibers embedded in ultra-high-performance concrete, Cement Concr. Compos. 49 (2014) 59–69.
[30] D.P. Bentz, K.A. Snyder, Protected paste volume in concrete: extension to internal curing using saturated lightweight fine aggregate, Cement Concr. Res. 29 (11) (1999) 1863–1867.
[31] A. Bentur, S.I. Igarashi, K. Kovler, Prevention of autogenous shrinkage in high-strength concrete by internal curing using wet lightweight aggregates, Cement Concr. Res. 31 (11) (2001) 1587–1591.
[32] S. Zhutovsky, K. Kovler, A. Bentur, Efficiency of lightweight aggregates for internal curing of high strength concrete to eliminate autogenous shrinkage, Mater. Struct. 35 (2002) 97–101.
[33] J. Castro, L. Keiser, M. Golias, J. Weiss, Absorption and desorption properties of fine lightweight aggregate for application to internally cured concrete mixtures, Cement Concr. Compos. 33 (10) (2011) 1001–1008.
[34] R. Henkensiefken, D. Bentz, T. Nantung, J. Weiss, Volume change and cracking in internally cured mixtures made with saturated lightweight aggregate under sealed and unsealed conditions, Cement Concr. Compos. 31 (7) (2009) 427–437.
[35] P. Lura, M. Wyrzykowski, C. Tang, E. Lehmann, Internal curing with lightweight aggregate produced from biomass-derived waste, Cement Concr. Res. 59 (2014) 24–33.
[36] X. Ma, J. Liu, C. Shi, A review on the use of LWA as an internal curing agent of high performance cement-based materials, Construct. Build. Mater. 218 (2019) 385–393.
[37] F. Rajabipour, G. Sant, J. Weiss, Interactions between shrinkage reducing admixtures (SRA) and cement paste's pore solution, Cement Concr. Res. 38 (5) (2008) 606–615.
[38] M. Wyrzykowski, P. Trtik, B. Münch, J. Weiss, P. Vontobel, P. Lura, Plastic shrinkage of mortars with shrinkage reducing admixture and lightweight aggregates studied by neutron tomography, Cement Concr. Res. 73 (2015) 238–245.
[39] J. Justs, M. Wyrzykowski, D. Bajare, P. Lura, Internal curing by superabsorbent polymers in ultra-high performance concrete, Cement Concr. Res. 76 (2015) 82–90.
[40] S.H. Kang, S.G. Hong, J. Moon, Importance of drying to control internal curing effects on field casting ultra-high performance concrete, Cement Concr. Res. 108 (2018) 20–30.
[41] O.M. Jensen, P.F. Hansen, Water-entrained cement-based materials: I. Principles and theoretical background, Cement Concr. Res. 31 (4) (2001) 647–654.
[42] N.V. Tuan, G. Ye, K.V. Breugel, Internal curing of ultra high performance concrete by using rice husk ash, in: Proceedings of the International RILEM Conference on Material Science, 2010, pp. 265–274. Aachen, Germany.
[43] V.T.A. Van, C. Rößler, D.D. Bui, H.M. Ludwig, Rice husk ash as both pozzolanic admixture and internal curing agent in ultra-high performance concrete, Cement Concr. Compos. 53 (2014) 270–278.
[44] S. Staquet, B. Espion, Early age autogenous shrinkage of UHPC incorporating very fine fly ash or metakaolin in replacement of silica fume, in: Proceedings of the International Symposium on Ultra-high-performance Concrete, Kassel, Germany, 2004, pp. 587–599.
[45] M.S.M. Norhasri, M.S. Hamidah, A.M. Fadzil, O. Megawati, Inclusion of nano metakaolin as additive in ultra high performance concrete (UHPC), Construct. Build. Mater. 127 (2016) 167–175.
[46] Y. Liu, Y. Wei, Effect of calcined bauxite powder or aggregate on the shrinkage properties of UHPC, Cement Concr. Compos. 118 (2) (2021) 103967.
[47] S. Kawashima, S.P. Shah, Early-age autogenous and drying shrinkage behavior of cellulose fiber-reinforced cementitious materials, Cement Concr. Compos. 33 (2) (2011) 201–208.
[48] R. Ma, L. Guo, S. Ye, W. Sun, J. Liu, Influence of hybrid fiber reinforcement on mechanical properties and autogenous shrinkage of an ecological UHPFRCC, J. Mater. Civ. Eng. 31 (5) (2019), 04019032.
[49] S.H. Kang, S.G. Hong, J. Moon, Shrinkage characteristics of heat-treated ultra-high performance concrete and its mitigation using superabsorbent polymer based internal curing method, Cement Concr. Compos. 89 (2018) 130–138.
[50] S.H. Kang, S.G. Hong, J. Moon, The use of rice husk ash as reactive filler in ultra-high performance concrete, Cement Concr. Res. 115 (2019) 389–400.
[51] B.J. Mohr, L. Premenko, H. Nanko, K.E. Kurtis, Examination of wood-derived powder and fibers for internal curing of cement-based materials, in: Proceedings of the 4th International Seminar on Self-Desiccation and its Importance in Concrete Technology, 2005, pp. 229–244. Gaithersburg, US.
[52] X. Wang, R. Yu, Z. Shui, Q. Song, Z. Zhang, Mix design and characteristics evaluation of an eco-friendly ultra-high performance concrete incorporating recycled coral based materials, J. Clean. Prod. 165 (2017) 70–80.
[53] J. Liu, Z. Ou, J. Mo, Y. Chen, T. Guo, W. Deng, Effectiveness of saturated coral aggregate and shrinkage reducing admixture on the autogenous shrinkage of ultrahigh performance concrete, Adv. Mater. Sci. Eng. (2017) 2703264, 2017.
[54] K. Liu, R. Yu, Z. Shui, X. Li, C. Guo, B. Yu, S. Wu, Optimization of autogenous shrinkage and microstructure for ultra-high performance concrete (UHPC) based on appropriate application of porous pumice, Construct. Build. Mater. 214 (2019) 369–381.
[55] K. Liu, R. Yu, Z. Shui, X. Li, X. Ling, W. He, S. Yi, S. Wu, Effects of pumice-based porous material on hydration characteristics and persistent shrinkage of ultra-high performance concrete (UHPC), Materials 12 (1) (2019) 11.
[56] W. Meng, K.H. Khayat, Effects of saturated lightweight sand content on key characteristics of ultra-high-performance concrete, Cement Concr. Res. 101 (2017) 46–54.
[57] J. Liu, C. Shi, N. Farzadnia, X. Ma, Effects of pretreated fine lightweight aggregate on shrinkage and pore structure of ultra-high strength concrete, Construct. Build. Mater. 204 (2019) 276–287.
[58] M. Valipour, K.H. Khayat, Coupled effect of shrinkage-mitigating admixtures and saturated lightweight sand on shrinkage of UHPC for overlay applications, Construct. Build. Mater. 184 (2018) 320–329.
[59] H. Huang, G. Ye, Examining the "time-zero" of autogenous shrinkage in high/ultra-high performance cement pastes, Cement Concr. Res. 97 (2017) 107–114.
[60] P. Shen, L. Lu, F. Wang, Y. He, S. Hu, J. Lu, H. Zheng, Water desorption characteristics of saturated lightweight fine aggregate in ultra-high performance concrete, Cement Concr. Compos. 106 (2020) 103456.
[61] X. Zhang, Z. Liu, F. Wang, Autogenous shrinkage behavior of ultra-high performance concrete, Construct. Build. Mater. 226 (2019) 459–468.
[62] O.M. Jensen, P.F. Hansen, Influence of temperature on autogenous deformation and relative humidity change in hardening cement paste, Cement Concr. Res. 29 (4) (1999) 567–575.
[63] A. Loukili, A. Khelidj, P. Richard, Hydration kinetics, change of relative humidity, and autogenous shrinkage of ultra-high-strength concrete, Cement Concr. Res. 29 (4) (1999) 577–584.
[64] B.A. Schrefler, C.E. Majorana, G.A. Khoury, D. Gawin, Thermo-hydro-mechanical modelling of high performance concrete at high temperatures, Eng. Comput. 19 (7) (2002) 787–819.
[65] I. Maruyama, A. Teramoto, Temperature dependence of autogenous shrinkage of silica fume cement pastes with a very low water-binder ratio, Cement Concr. Res. 50 (2013) 41–50.
[66] ASTM C1761-09, Standard Specification for Lightweight Aggregate for Internal Curing of Concrete, 2009.
[67] R. Yu, P. Spiesz, H.J.H. Brouwers, Mix design and properties assessment of ultra- high performance fibre reinforced concrete (UHPFRC), Cem. Concr. Res. 56 (2014) 29–39.
[68] P.S. Mangat, M.M. Azari, A theory for the free shrinkage of steel fibre reinforced cement matrices, J. Mater. Sci. 19 (1984) 2183–2194.
[69] B. Zhou, Y. Uchida, Influence of flowability, casting time and formwork geometry on fiber orientation and mechanical properties of UHPFRC, Cement Concr. Res. 95 (2017) 164–177.
[70] E. Gallucci, P. Mathur, K. Scrivener, Microstructural development of early age hydration shells around cement grains, Cement Concr. Res. 40 (1) (2010) 4–13.

[71] P.C. Aïtcin, High Performance Concrete, CRC press, 2011.
[72] O.M. Jensen, P.F. Hansen, Water-entrained cement-based materials: II. Experimental observations, Cem. Concr. Res. 32 (6) (2002) 973–978.
[73] P. Mounanga, V. Baroghel-Bouny, A. Loukili, A. Khelidj, Autogenous deformations of cement pastes: Part I. Temperature effects at early age and micro–macro correlations, Cement Concr. Res. 36 (1) (2006) 110–122.
[74] A. Quennoz, K.L. Scrivener, Interactions between alite and C3A-gypsum hydrations in model cements, Cement Concr. Res. 44 (2013) 46–54.
[75] I.D.L. Varga, B.A. Graybeal, Dimensional stability of grout-type materials used as connections between prefabricated concrete elements, J. Mater. Civ. Eng. 27 (9) (2015), 04014246.
[76] A. Korpa, T. Kowald, R. Trettin, Phase development in normal and ultra high performance cementitious systems by quantitative X-ray analysis and thermoanalytical methods, Cement Concr. Res. 39 (2) (2009) 69–76.
[77] B.J. Mohr, K.L. Hood, Influence of bleed water reabsorption on cement paste autogenous deformation, Cement Concr. Res. 40 (2) (2010) 220–225.
[78] Z.C. Grasley, D.A. Lange, Thermal dilation and internal relative humidity of hardened cement paste, Mater. Struct. 40 (2007) 311–317.
[79] K. Meinhard, R. Lackner, Multi-phase hydration model for prediction of hydration-heat release of blended cements, Cement Concr. Res. 38 (6) (2008) 794–802.
[80] B. Lothenbach, K. Scrivener, R.D. Hooton, Supplementary cementitious materials, Cement Concr. Res. 41 (2011) 1244–1256.
[81] S. Dittrich, J. Neubauer, F.G. Neunhoeffer, The influence of fly ash on the hydration of OPC within the first 44 h-A quantitative in situ XRD and heat flow calorimetry study, Cement Concr. Res. 56 (2014) 129–138.
[82] S. Chithiraputhiran, N. Neithalath, Isothermal reaction kinetics and temperature dependence of alkali activation of slag, fly ash and their blends, Construct. Build. Mater. 45 (2013) 233–242.
[83] N.K. Lee, K.T. Koh, M.O. Kim, G.S. Ryu, Uncovering the role of micro silica in hydration of ultra-high performance concrete (UHPC), Cement Concr. Res. 104 (2018) 68–79.
[84] B. Lothenbach, D. Rentsch, E. Wieland, Hydration of a silica fume blended low-alkali shotcrete cement, Phys. Chem. Earth 70–71 (2014) 3–16.
[85] B. Lothenbach, D.A. Kulik, T. Matschei, M. Balonis, L. Baquerizo, B. Dilnesa, G.D. Miron, R.J. Myers, Cemdata18: a chemical thermodynamic database for hydrated Portland cements and alkali-activated materials, Cement Concr. Res. 115 (2019) 472–506.
[86] M. Wyrzykowski, P. Lura, F. Pesavento, D. Gawin, Modeling of internal curing in maturing mortar, Cement Concr. Res. 41 (2011) 1349–1356.
[87] S. Zhutovsky, K. Kovler, Hydration kinetics of high-performance cementitious systems under different curing conditions, Mater. Struct. 46 (2013) 1599–1611.
[88] X. Hu, C. Shi, Z. Shi, B. Tong, D. Wang, Early age shrinkage and heat of hydration of cement-fly ash-slag ternary blends, Construct. Build. Mater. 153 (2017) 857–865.
[89] A.M. Soliman, M.L. Nehdi, Effect of partially hydrated cementitious materials and superabsorbent polymer on early-age shrinkage of UHPC, Construct. Build. Mater. 41 (2013) 270–275.
[90] J. Kaufmann, F. Winnefeld, D. Hesselbarth, Effect of the addition of ultrafine cement and short fiber reinforcement on shrinkage, rheological and mechanical properties of Portland cement pastes, Cement Concr. Compos. 26 (5) (2004) 541–549.
[91] P.C. Aïtcin, Autogenous Shrinkage Measurement, Proceedings of the International Workshop on Autogenous Shrinkage of Concrete, Hirosima, Japan, 1998, pp. 245–256.